Korean J. Chem. Eng., 37(1), 159-165 (2020)
DOI: 10.1007/s11814-019-0430-8

pISSN: 0256-1115
eISSN: 1975-7220

Study of mercury-adsorption behavior in the exhaust gas of KI-impregnated ACF

In-Soo Kang*, Yo-Seob Shin*, Byung Chan Kwon*, No-Kuk Park*,†, Tae Jin Lee*, Seung Woo Lee*,†, and Myung Jo Seo**

*School of Chemical Engineering, Yeungnam University, 280 Daehak-ro, Gyeongsan, Gyeongbuk 38541, Korea
**Micro-one Inc., 368 Yeongok-road, Ibjang-myeon, Seobuk-gu, Cheonan-si, Chungnam 31026, Korea
(*Received 6 August 2019 • accepted 12 November 2019*)

Abstract−This study examined the selective removal of gaseous mercury contained in combustion flue gas by potassium iodide (KI) loaded on activated carbon fibers (ACF). Activated carbon, such as ACF, although a useful mercury sorbent, shows poor performance in the direct treatment of high-temperature flue-gases because it removes mercury only by physical adsorption. KI can remove mercury at high temperatures via a gas-solid reaction between mercury and adsorbents, and it has been confirmed experimentally that it shows high mercury removal performance in the temperature range of 100-200 °C. On the other hand, KI in the absence of a porous support with a high surface area has low mercury-adsorption removal efficiency. Hence, a high surface area support is needed for adsorption removal. In the present study, mercury contained in combustion exhaust gas could be removed efficiently using KI as an adsorption activity enhancer on an activated carbon fiber (ACF), which provided a high surface area.

Keywords: Mercury Adsorption, KI-impregnated ACF, High Temperature Hg Removal, Incineration Exhaust Gas Treatment

INTRODUCTION

Recently, the problem of ultrafine dust has been highlighted as a social issue worldwide. The formation of ultrafine dust has a range of causes, including nitrogen oxides (NOx), sulfur oxides (SOx), volatile organic compounds (VOCs), and particulate matter generated in combustion processes, such as energy production and environmental facilities [1]. These materials act as precursors for generating aerosolized ultrafine dust [2]. To remove the precursors of ultrafine dust discharged from the combustion process, it is important to upgrade the denitration, desulfurization, and dust collection techniques. The dust-collecting technique for removing the particulate matter generated in the combustion process can be classified into two procedures: exhaust gas-cleaning techniques, such as a wet scrubber, and trapping techniques, such as a bag filter and electrostatic precipitator [3,4]. The techniques for enhancing dust collection technology using a bag filter have been developed by adding a membrane filter to remove ultrafine dust as well as heavy metals, such as mercury [5-7].

Most studies have focused on removing mercury in the gas phase using activated carbon because of its high surface area and low cost. Despite the high surface area (approximately 500 m^2/g) of activated carbon, however, studies have been carried out to support iodine, chlorine, and sulfur on the surface of activated carbon because of the low adsorption capacity of mercury. Iodine, chlorine, and sulfur have low mercury adsorption capacity when used alone. However, they have improved adsorption capacity and are capable of selective removal when supported on a high surface area support [8,9]. According to Seo et al., the surface of activated carbon has been reported to lose chlorine at temperatures greater than 100 °C [9]. In addition, sulfur supported on the surface of activated carbon may be lost by forming SOx under high-temperature exhaust gas conditions, where oxygen is present. Therefore, iodine is advantageous as a stable mercury-adsorbed species in the relatively high-temperature region.

This study examined the removal performance of gaseous mercury in activated carbon fibers (ACF) as a preliminary study focusing on the addition of ACFs to a filter material and achieving an adsorption removal function of a gas phase heavy metal using a PTFE membrane filter. The activated carbon material has a high surface area and excellent adsorption characteristics for heavy metals. ACFs were applied as a support for adsorption because of their favorable results when added to a bag filter. Most of the adsorbent for adsorbing and removing mercury is in a packed bed. Porous metal oxides, such as activated carbon, zeolite, and porous alumina impregnated with Cu, are used in commercial facilities [7,10]. On the other hand, these facilities are operated for the treatment of relatively high concentrations of mercury, and the capacity of these facilities is considerably large. The equipment used to remove trace amounts of mercury is too large for general use. Therefore, in these processes, it is important to develop high-precision purification technology for adsorbing and removing trace amounts of gaseous mercury after a considerable amount of mercury has been adsorbed and removed.

This study compared the mercury removal performance of adsorbents loaded with KI on the surface of the ACF as well as the performance according to the adsorption temperature. In addition, the effects of the KI loading were investigated.

EXPERIMENTS

1. Materials

ACFs were used as a porous material for mercury adsorption.

†To whom correspondence should be addressed.
E-mail: leesw1212@ynu.ac.kr

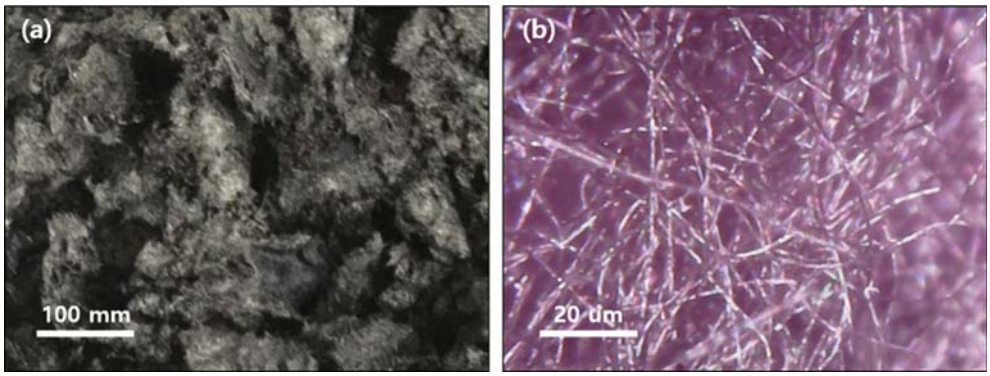

Fig. 1. Optical microscopy images of ACF foam, (a) digital camera image and (b) magnified image x 600.

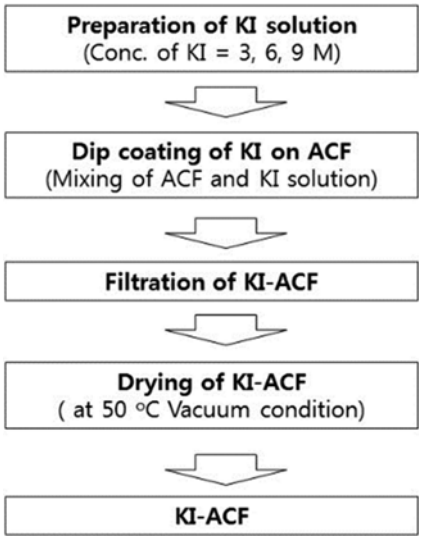

Fig. 2. Preparation procedure of the KI-ACF adsorbents.

The material was mixed with water, disassembled in a rotary wet pulverizer and dried. A sheet-like ACF nonwoven fabric was disassembled in the form of wool in the pulverizing process, as shown in Fig. 1. The surface area of the ACF (STF-1150, commercial product supplied in Korea Activated Carbon Fiber Ltd.) used in the experiment, was approximately 1,150 m^2/g, and the pore volume and mean pore diameter were approximately 0.623 cm^3/g and 20 A, respectively.

KI was used to improve the adsorption performance of the ACF. As shown in Fig. 2, an aqueous KI solution was prepared for dip coating. The concentration of the KI solution for a sufficient KI loading on the ACF surface via dip coating was 3, 6, and 9 M, which is denoted as KI-ACF3, KI-ACF6, and KI-ACF9, respectively. The ACFs were immersed in the KI solution prepared at different concentrations and left to stand for 24 h. Subsequently, the ACFs were filtered through a filter net, separated from the KI solution, and vacuum dried at 50 °C at approximately 0.09 kg_f/m^2.

The dried ACF adsorbent was stored in a vacuum desiccator to prevent the absorption of moisture. The adsorbent was weighed in small quantities and used for the mercury adsorption tests after packing into an adsorption column.

2. Hg Adsorption Tests

Fig. 3 presents the setup for the mercury adsorption experiment using ACF. The experimental setup for the mercury adsorption tests consisted of a Hg evaporator for mercury vapors, an adsorption column filled with ACF, mercury analyzer (Mercury Instrument, VM3000 Mercury Vapor Monitor), and mercury absorption bottle (4% $KMnO_4$/10% H_2SO_4 mixed solution). The mercury absorption bottle was used to remove mercury prior to discharge to the atmosphere. Nitrogen gas was used as a carrier gas to transfer mercury vapor from the mercury evaporator to the adsorption column. Nitrogen gas was supplied directly to the mercury evaporator and divided into tubing for transfer and for controlling the mercury concentration. Nitrogen was supplied at a flow rate of approximately

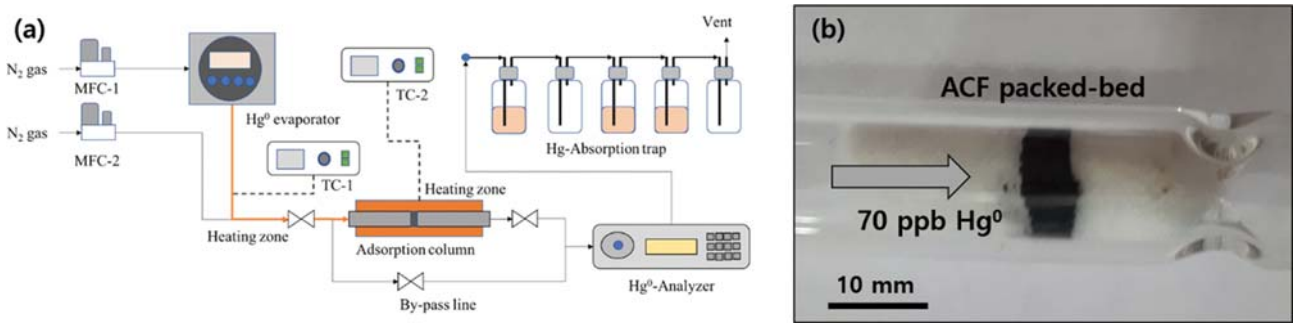

Fig. 3. Schematic diagram of the experimental apparatus and adsorbent packing column for the Hg adsorption tests, (a) schematic diagram and (b) column image.

200 ml/min to a mercury evaporator for gas phase mercury transport, and nitrogen was supplied to the mercury evaporator downstream at a flow rate of approximately 1,500 ml/min to control the mercury concentration. The mercury evaporator was equipped with a permeation tube filled with liquid mercury, and the mercury was diffused through the permeation tube to the outside according to the heating temperature. When the heating temperature of the permeation tube was heated to 90 °C and the total nitrogen flow rate was 1,700 ml/min, mercury was supplied to the adsorption column at a concentration of approximately 70 ppb. All mercury adsorption tests conducted in this study were carried out by introducing 70 ppb of mercury to the adsorption column. In addition, a mercury-only analyzer connected directly to the outlet of the adsorption column was equipped to measure the mercury concentration during the adsorption experiment. The tubing from the mercury evaporator to the inlet of the adsorption column was heated to 130 °C using a heating band to prevent the physical adsorption of mercury inside. To measure the adsorption time accurately, the mercury-containing nitrogen gas was passed through the by-pass line until the adsorption experiment started. In the mercury adsorption experiment of the ACF, the adsorption column was packed with approximately 0.1 g of ACF, and the flow of nitrogen gas containing 70 ppb of mercury passing through the by-pass line was switched to the adsorption column. The mercury concentration in the outlet of the adsorption column was measured to obtain a breakthrough curve. Finally, the adsorption column was heated using a heating band to examine the adsorption behavior of the ACF according to the temperature. The heating temperature was controlled by inserting a thermocouple inside the adsorption-bed and connecting it to a temperature controller.

3. Characterization of the ACF Adsorbent

To measure the surface area of the adsorbent, the surface and pore characteristics of the ACF were measured using a nitrogen adsorption instrument (Micromeritics, ASAP2020) and the surface composition was measured by scanning electron microscopy/energy dispersive X-ray spectrometry (SEM/EDX, S-4100, Hitachi, Japan).

RESULTS AND DISCUSSION

1. Effects of the KI-impregnation by Dip Coating

The adsorption characteristics of mercury on the ACF and KI-ACF samples, which is KI-loaded ACF, were investigated at room temperature. The Hg-breakthrough curves showed that the mercury adsorption behavior of the ACF and KI-ACF samples was significantly different, as shown in Fig. 4. The mercury-adsorption breakthrough curves of the ACF sample revealed the mercury concentration to increase gradually, as shown in Fig. 4(a). After a certain time, the concentration of mercury at the outlet of the adsorption column increased sharply compared to the inflow concentration. As shown in Fig. 4(b), the Hg-breakthrough curve of KI-ACF6 revealed mercury after 50 min. The mercury concentration increased gradually and was absorbed sustainably in the KI-ACF6 packed-bed until 600 min, which was the experimental time. The tendency of the mercury breakthrough curve confirmed the mercury adsorption behavior of KI loaded on ACF. In addition, the adsorption sites of the KI-ACF were larger than the adsorption sites on the ACF surfaces without KI, which indicates more effective adsorption sites for the removal of mercury. The slope of the breakthrough curve in Fig. 4(a) and (b) showed a high adsorption rate on the adsorption sites of ACF, whereas the adsorption rate was relatively low on the adsorption sites of KI-loaded ACF. The process of gaseous mercury adsorption using a solid adsorbent can be considered the result of an interaction between the solid and gas. A large number of adsorption sites and a strong adsorption intensity are required to remove the gas phase material at a certain concentration with high efficiency. As the number of available adsorption sites decreases, adsorption is terminated within a short time, so that the slope of the breakthrough curve tends to rise sharply. On the other hand, if there are a large number of available adsorption sites with low adsorption strength, adsorption can proceed for a long time, despite the low level of removal by adsorption. Hence, high adsorption can be achieved. In the case of KI-ACF, the adsorption rate was relatively low at room temperature, but a high level of adsorption was achieved. Based on these results, it was concluded that the predominant adsorption behavior of ACF and KI-ACF was physical and chemical adsorption, respectively.

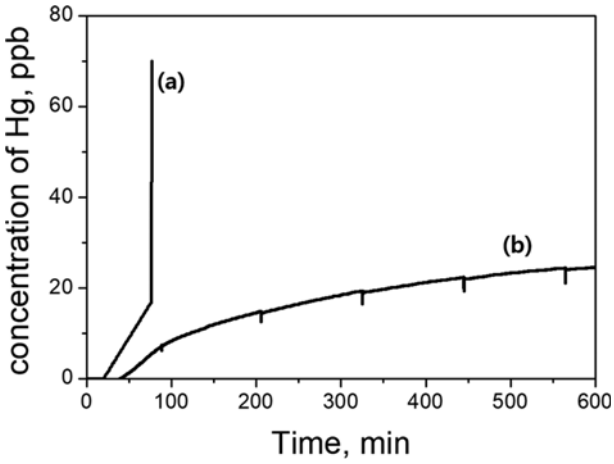

Fig. 4. Hg breakthrough curves in the Hg adsorption tests for the ACF and KI-ACF samples, (a) ACF and (b) KI-ACF6.

The mercury adsorption behavior of KI-ACF changed according to the concentration of the aqueous KI solution used for the ACF dip coating. As shown Fig. 5, the amount of mercury adsorption by KI-ACF6 was higher than that of KI-ACF3. The order of the mercury concentration at the outlet was KI-ACF3>KI-ACF6>KI-ACF9. These results suggest that the content of KI loaded on the ACF surfaces increased with increasing concentration of the aqueous KI solution for a dip-coating. The KI-ACF9 was subjected to a long-term adsorption test for approximately 37 h. As a result, the outflow concentration of mercury supplied to the adsorption column at a concentration of 70 ppb was maintained at approximately 10 ppb. The efficiency of mercury removal in this test was approximately 86%. The long-term adsorption and efficient mercury removal may arise from the low adsorption strength of adsorption sites as well as the weak gas-solid interaction, as mentioned above.

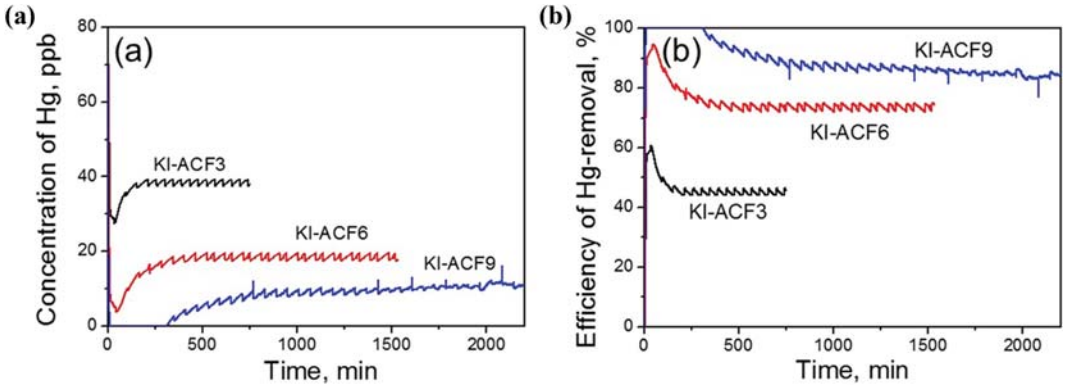

Fig. 5. Hg breakthrough curves in the Hg adsorption tests for the KI-ACF3, KI-ACF6, and KI-ACF9 sample.

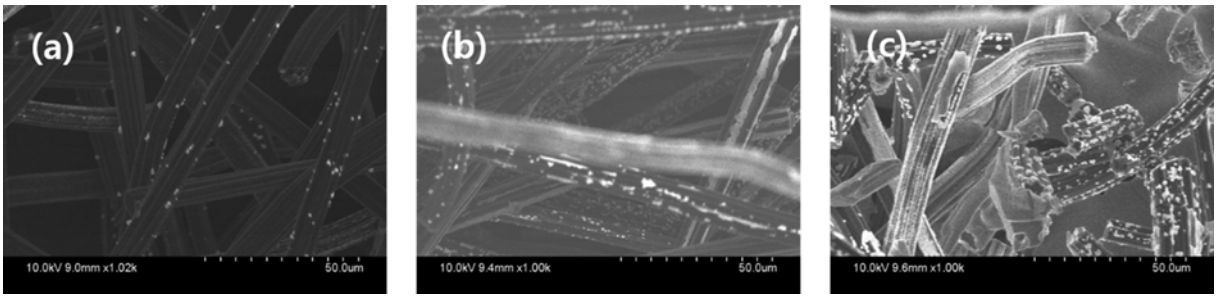

Fig. 6. SEM images of the ACF samples coated with a KI solution of various concentrations for measurements of the KI loading by EDX analysis, (a) KI-ACF3, (b) KI-ACF6, and (c) KI-ACF9.

2. Characterization of the KI-ACF Adsorbents: N_2-adsorption Method and SEM/EDX Analysis

As shown in Fig. 5, the level of mercury adsorption on the KI-ACF adsorbents in the mercury adsorption experiment changed according to the concentration of the aqueous KI solution used as the dip-coating agent. The content of KI on the surface of the three KI-ACF adsorbents prepared with the aqueous KI solutions at different concentrations was analyzed by SEM/EDX. As shown in Fig. 6, there were significant changes in the morphology of the surface of the KI-ACF samples caused by a change in the concentration of the aqueous KI solution used in the dip coating process. As the concentration of KI increased, the loading amount of KI on the surface of the ACF was clearly observed to increase, and it was confirmed that KI-ACF9, a sample coated in the 9 M KI aqueous solution, had a very uniform coating. On the other hand, EDX analysis confirmed that KI was loaded on the ACF sample, and the content of KI on the ACF was changed. As shown in Table 1, the content of KI on the ACF surface increased with increasing aqueous KI solution concentration used to support KI. EDX analysis revealed a difference in the K and I content. The theoretical K/I atomic weight ratio in potassium iodide is approximately 0.308 in terms of stoichiometry. On the other hand, after KI was loaded on the ACF with an aqueous KI solution by dip coating, the content of I on the surface of the KI-ACF sample was higher than that of K. In particular, the K/I weight ratio on the surface of the KI-ACF3 was significantly low, approximately 0.062. The K/I weight ratio on the surface of the KI-ACF6 and KI-ACF9 was approximately 0.105 and 0.295, respectively. These results suggest that K^+ and I^- ions in the aqueous solution are adsorbed on the surface of the ACF. In particular, as shown in this study, when KI-ACF was prepared by dip coating, the amount of adsorption on the ACF surface could be altered by the adsorption characteristics of ions in the aqueous solution. As described above, the level of mercury adsorption due to the KI loading tends to increase, even though iodide ions are supported better and the amount of potassium ions is low. This suggests that the I^- acts as an effective adsorption site for mercury adsorption.

As shown in Fig. 7(a), the amount of iodine on the surface of

Table 1. Elemental composition of ACF coated with a KI solution at various concentrations by EDX analysis

Concentration of KI solution	Elemental composition of ACF coated with a KI solution using a dip coating method, wt%				K/I ratio
	C	K	I	Total	
3.0 M	96.03	0.23	3.74	100	0.062
6.0 M	87.21	1.21	11.58	100	0.105
9.0 M	76.07	5.46	18.48	100	0.295

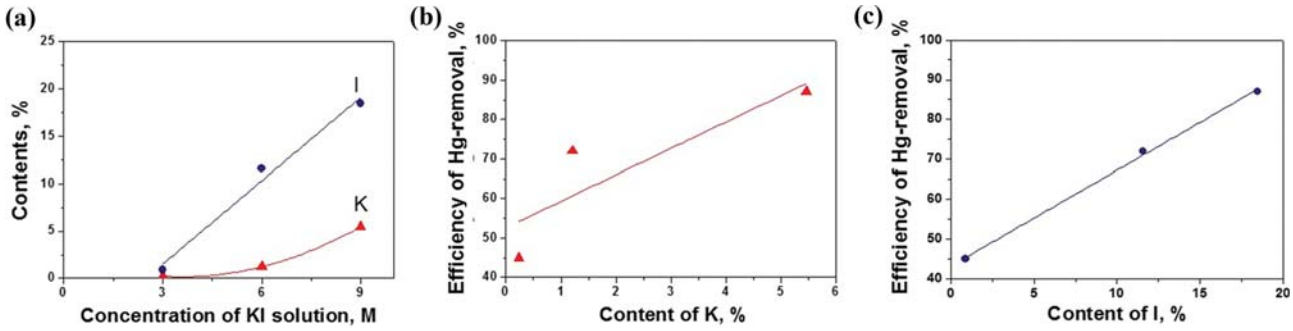

Fig. 7. Correlation curves, (a) content of K and I on the surface of KI-ACF according to the aqueous KI solution concentration, (b) correlation between the mercury adsorption performance and K content, (c) correlation between the mercury adsorption performance and I content.

the KI-ACF adsorbent increased linearly with increasing KI concentration in the aqueous solution during dip coating, whereas the potassium concentration increased nonlinearly. Fig. 7(b) and 7(c) show the correlation between the mercury removal efficiency of the dip-coated KI-ACF adsorbent and the content of potassium and iodine on the KI-ACF adsorbent according to the concentration of the aqueous KI solution. This confirmed that the content of potassium was non-linear, whereas the iodine content was linear. The iodine content is the main activation species affecting the efficiency of mercury adsorption.

In contrast, the surface area of the three KI-ACF samples determined using the nitrogen adsorption method decreased slightly with increasing KI loading, as shown in Table 2. On the other hand, no significant decrease in surface area was observed, regardless of the concentration of the aqueous KI solution for dip coating. This indicates that the KI adsorbent was effectively loaded on the ACF surface by dip coating. In the case of a forcible loading, such as a vacuum rotary evaporation, which is generally used as an impregnation method, KI blocks the pores of the ACF, which causes micropore plugging [11]. In the case of dip coating, however, the loading was small, and no decrease in pore volume was observed. Therefore, the adsorbent function can be maintained because the high surface area of the ACF can be preserved. If the mercury adsorption capacity were increased, it would be necessary to identify the optimal conditions for increasing the loading of KI and minimizing the decrease in surface area of the KI-ACF adsorbent.

Table 2. Surface and pore properties of the KI-ACF samples measured using the N_2 adsorption method

Properties	Concentration of KI in dip coating process		
	3 M	6 M	9 M
Single point surface area, m^2/g	1044.8	916.2	976.9
BET surface area, m^2/g	1020.8	894.5	956.2
t-Plot micropore area, m^2/g	896.6	754.4	802.6
t-Plot external surface area, m^2/g	124.2	140.1	153.6
BJH-ads. surface area, m^2/g	53.2	71.5	80.5
BJH-des. surface area, m^2/g	62.4	88.0	97.7
Single point total pore volume, cm^3/g	0.5303	0.4819	0.5167
t-Plot micropore volume, cm^3/g	0.4629	0.3910	0.4148
BJH-ads. pore volume, cm^3/g	0.0343	0.0577	0.0664
BJH-des. pore volume, cm^3/g	0.0379	0.0637	0.0728
Ave. pore width, nm	2.08	2.15	2.16
BJH-ads. pore diameter, nm	2.58	3.23	3.30
BJH-des. pore diameter, nm	2.43	2.89	2.98

3. Effects of the Adsorption Temperature

The adsorption behavior of KI-ACF was investigated according to the temperature of the adsorption column, considering that the temperature of the combustion exhaust gas ranged from 150 to 250 °C. The adsorption temperature was maintained at 50, 100, 150, and 200 °C. In this mercury adsorption test, KI-ACF6, which showed relatively high performance, was used. The Hg breakthrough time increased with increasing adsorption temperature up to 150 °C, as shown in Fig. 8. Table 3 lists the mercury adsorption capacity of KI-ACF according to the breakthrough time. Fig. 8 shows the breakthrough time of mercury observed from the mercury concentration in the outlet of the adsorption column according to the adsorption temperature. The increase in mercury adsorption rate with increasing temperature means that the adsorption strength increased, which means that the adsorption of KI-ACF and Hg in the gas phase depends on chemisorption. Thus, mercury was adsorbed on the surface of KI-ACF via a chemical reaction, and the rate of adsorption via a chemical reaction increased with increasing temperature according to the Arrhenius equation [12]. This means that Hg and I were adsorbed chemically in the form of HgI by a chemical reaction. The adsorption capacity of mercury increased sharply at 150 °C. The increase in adsorption capacity and adsorption rate with increasing temperature also means that KI loaded on the ACF surface was adsorbed chemically by the gas-solid reaction. Chemisorption requires an adequate adsorption energy to cause the adsorbate to interact with the adsorbent. On the other hand, the amount of adsorption by physical adsorption decreased with increasing temperature. Moreover, when the temperature was excessively high, the desorption of chemically adsorbed mercury and the degradation of adsorption due to the decomposition of chemically bound mercury could also occur. As shown in Table 3, the lower amount of adsorption at 200 °C than at 150 °C can be attributed to these reasons.

The mercury adsorption capacity of the KI-ACF6 adsorbent on the temperature of the exhaust gas can be obtained with the cor-

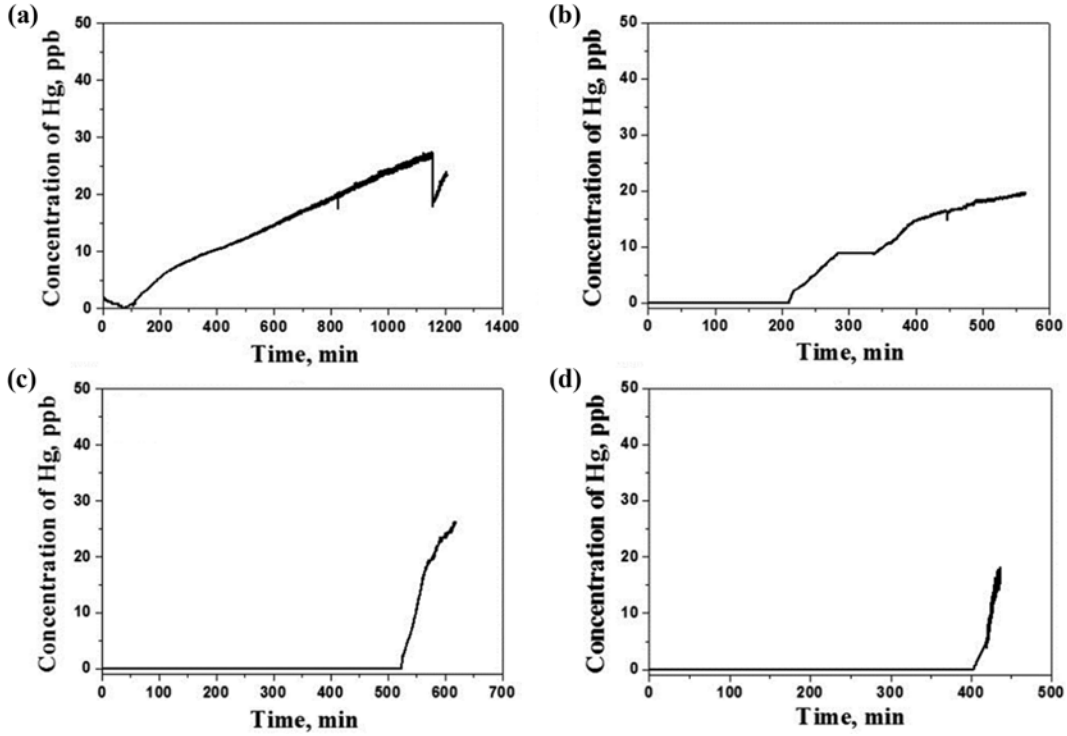

Fig. 8. Hg breakthrough curves in Hg adsorption tests at various adsorption temperatures for KI-ACF samples coated with a 6.0 M KI solution, (a) 50 °C, (b) 100 °C, (c) 150 °C, and (d) 200 °C.

Table 3. Hg breakthrough time and Hg capacity of KI-ACF according to the adsorption temperature

Adsorption temperature, °C	Hg breakthrough time, min	Hg capacity, mgHg/g-sorbent
25	49	0.53
50	125	1.35
100	180	1.95
150	525	5.68
200	470	5.08

relation curve, as shown in Fig. 9. As described above, the mercury adsorption capacity tended to increase with increasing temperature, and showed a second-order function correlation with temperature. In this study, the correlation between the exhaust gas temperature and the mercury adsorption capacity of KI-ACF6 adsorbent was proposed, as shown in Eq. (1).

$$\text{Mercury removal efficiency } (mgHg^0/g \text{ sorbents}) = 35.75 - 0.2267T + 0.004T^2 \quad (1)$$

To observe the desorption behavior of adsorbed mercury, the desorption behavior of mercury from the ACF and KI-ACF6 samples, which had adsorbed mercury at room temperature, was examined as a function of temperature under a nitrogen gas stream. The mercury concentration in the outlet of the adsorption column was measured during the mercury desorption tests. As shown in Fig. 10, the mercury desorption behavior of the ACF and KI-ACF6 showed a clear difference. In the case of ACF, mercury was desorbed to a concentration of above 10 ppb immediately after the start of

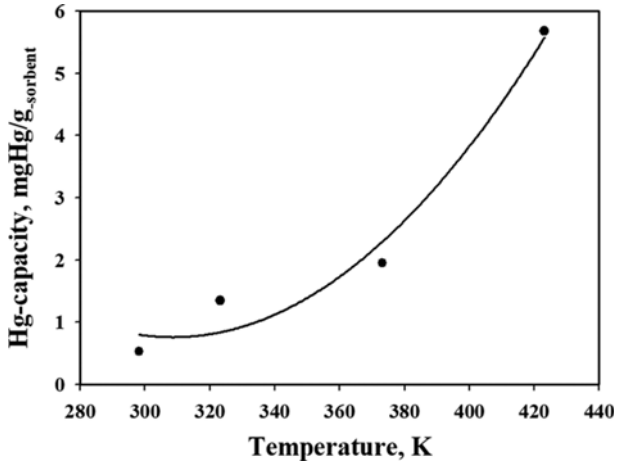

Fig. 9. Correlation curve between the Hg-removal capacity vs. temperature of exhaust gas on KI-ACF6 sorbent.

the desorption test. The amount of mercury desorbed increased from 140 °C, and the amount desorbed increased rapidly to 35 ppb after 225 °C. In the case of KI-ACF6, mercury was desorbed at concentrations lower than 10 ppb at room temperature, and the amount of mercury desorbed increased at 140 °C but decreased at 170 °C. The maximum mercury desorption concentration was less than 15 ppb. The desorption of adsorbed mercury increased with increasing temperature for ACF. In the case of KI-ACF6, the desorption of mercury was observed, but most of the mercury remained in the adsorbed state. In this way, the desorption behavior of the adsorbed mercury according to temperature was different because

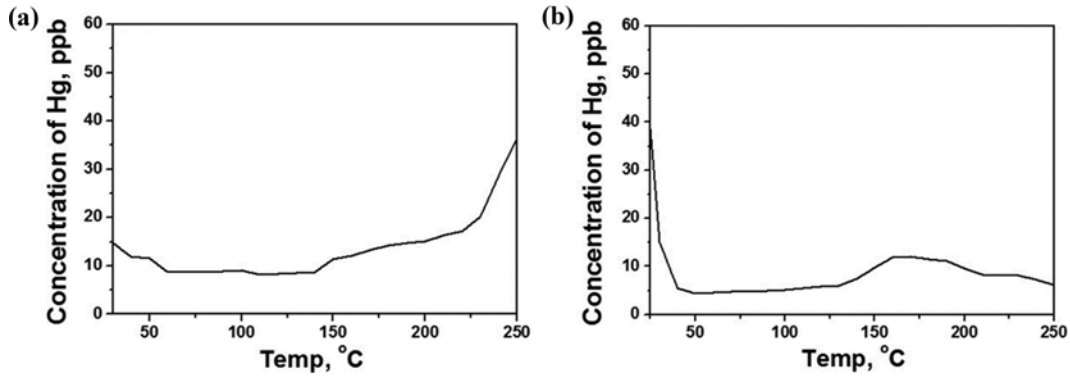

Fig. 10. Hg profiles by the desorption of Hg adsorbed on ACF and KI-ACF samples with increasing temperature, (a) ACF and (b) KI-ACF prepared with 6.0 M KI solution.

the ACF adsorbs mercury by physical adsorption, whereas KI-ACF adsorbs mercury by chemisorption. Overall, ACF is useful as an adsorbent to provide a large surface area, and KI supported on the surface of the ACF can act as an active material for enhancing the adsorption strength.

CONCLUSIONS

ACF and KI-ACF were applied to adsorb and remove mercury from exhaust gas. The mercury adsorption performance of ACF was improved by impregnating KI on the ACF by dip coating. In addition, when mercury was adsorbed using KI-ACF as an adsorbent, the adsorption efficiency of mercury increased with increasing temperature. This is because the KI component loaded on the surface of ACF adsorbs mercury chemically. The adsorption strength is a very important factor for adsorbing and removing mercury in the gas phase using a solid adsorbent, and KI acts as an active species for increasing the adsorption strength, which is due to the adsorption behavior corresponding to the chemical bond. Therefore, to maintain the high surface area of the adsorbent, an adsorbent such as ACF may be applied and the active species for increasing the adsorption strength may be supported on the surface of the adsorbent to improve the performance. In the future, it may be possible to remove trace amounts of mercury precisely by using a filtration and dust-collecting process by adding KI-supported ACF to the surface of a PTFE membrane filter.

ACKNOWLEDGEMENTS

This study was supported by the Korea Institute of Energy Technology Evaluation and Planning (KETEP) and the Ministry of Trade, Industry & Energy (MOTIE) of the Republic of Korea (No. 20161120200170).

REFERENCES

1. C. H. Song, C. M. Kim, Y. J. Lee, G. R. Carmichael, B. K. Lee and D. S. Lee, *J. Geophys. Res.*, **112**, D18206 (2007).
2. K. Maxwell-Meier, R. Weber, C. Song, D. Orsini, Y. Ma, G. R. Carmichael and D. G. Streets, *J. Geophys. Res.*, **109**, D19S07 (2004).
3. M. Chin, T. Diehl, P. Ginoux and W. Malm, *Atmos. Chem. Phys.*, **7**, 5501 (2007).
4. L.-M. Lo, D.-R. Chen and D. Y. H. Pui, *Powder Technol.*, **197**, 141 (2010).
5. K. Gai, A. Avellan, T. P. Hoelen, F. Lopez-Linares, E. S. Hatakeyama and G. V. Lowry, *Water Res.*, **157**, 600 (2019).
6. J.-H. Sung, S.-K. Back, E.-S. Lee, H.-N. Jang, Y.-C. Seo, Y.-S. Kang and M.-H. Lee, *J. Environ. Sci.*, **80**, 58 (2019).
7. K. C. Galbreath and C. J. Zygarlicke, *Fuel Process. Technol.*, **65**, 289 (2000).
8. S. J. Lee, Y.-C. Seo, J. Jurng and T. G. Lee, *Atmos. Environ.*, **38**, 4887 (2004).
9. H.-N. Jang, S.-K. Back, J.-H. Sung, B.-M. Jeong, Y.-S. Kang, C.-K. Lee, J. Jurng and Y.-C. Seo, *Korean J. Chem. Eng.*, **34**(3), 806 (2017).
10. L. Tong, T. Yue, P. Zuo, X. Zhang, C. Wang, J. Gao and K. Wang, *Fuel*, **197**, 1 (2017).
11. J. Kim, J. Y. Do, K. Nahm, N.-K. Park, J. Chi, J.-P. Hong and M. Kang, *Sep. Purif. Technol.*, **211**, 421 (2019).
12. N.-K. Park, B. C. Kwon, C. J. Park, M. Kang, T. J. Lee, S. J. Lee and J. H. Chi, *J. Nanosci. Nanotechnol.*, **19**, 6641 (2019).